

First-Principles Studies on Structural, Electronic and Optical Properties of Fe-doped NiS₂ Counter Electrode for Dye-Sensitised Solar Cells using DFT+U

N.A. Malik^{1,5}, N.N. Alam^{1,5}, M.H. Samat⁵, M.Z. Mohyedin^{1,5}, N.H. Hussin²,
O.H. Hassan^{3,5}, M.Z.A. Yahya^{4,5}, M.F.M. Taib^{1,5*}

¹Faculty of Applied Sciences, Universiti Teknologi MARA, 40450 Shah Alam, Selangor, Malaysia

²Faculty of Applied Sciences, Universiti Teknologi MARA, 26400 Jengka, Pahang, Malaysia

³Faculty of Arts and Design, Universiti Teknologi MARA, 40450 Shah Alam, Selangor, Malaysia

⁴Faculty of Defence Science & Technology, Universiti Pertahanan Nasional Malaysia, 57100 Kuala Lumpur, Malaysia

⁵Tonic Materials and Devices (iMADE), Institute of Science, Universiti Teknologi MARA, 40450 Shah Alam, Selangor, Malaysia

*Corresponding author's e-mail: mfariz@uitm.edu.my

Received: 3 July 2020

Accepted: 12 August 2020

Online First: 25 August 2020

ABSTRACT

The structural, electronic, and optical properties of nickel disulfide (NiS₂) and iron (Fe)-doped NiS₂ were computed by using first-principles calculations through the density functional theory (DFT) method. The Fe was used as a dopant element to understand the behaviour and the key mechanism of Fe-doped NiS₂ as a counter electrode in dye-sensitised solar cells (DSSC). The results indicated that the structural properties of the NiS₂ as the cubic crystal structure with the space group Pa $\bar{3}$ (205) (pyrite structure type) agree with experimental data. The density of states (DOS) of NiS₂ and Fe-doped NiS₂ shows a gapless bandgap due to Mott-Hubbard insulator behavior. As for optical properties, the optical absorption of NiS₂ is shifted towards the infrared (IR) region when doping with Fe while the conductivity of Fe-doped NiS₂ is slightly higher in conductivity. These optical properties show that Fe-doped NiS₂ is suitable for the photocatalytic activity and may provide an excellent electron charge transfer for a counter electrode in DSSC.



Keywords: *counter electrode; density functional theory; structural properties; electronic properties; optical properties.*

INTRODUCTION

Over the past few decades, a dye-sensitised solar cell (DSSC) has been discovered as a next-generation solar cell and promises a great potential device of renewable energy due to its cost-effective, simple manufacturing process and nontoxicity. As one of the most essential parts in DSSC, the counter electrode acts as a catalyst in regenerate redox mediator [1-4]. The counter electrode serves a crucial role with other components in producing electricity from the harvested sun [5]. Among all counter electrode materials, platinum (Pt) act as one of the most excellent counter electrodes which have been studied extensively because of its high electrochemical activity in reducing triiodide (I_3^-) [6]. Nevertheless, Pt has a disadvantage such as high cost and easily undergoes corrosion in the electrolytes due to the presence of redox mediators whereby limits the long-term stability of the counter electrode and may inflate the overall cost of DSSC [7-9].

Hence, the substitution of Pt counter electrode by other cost-effective materials that will exhibit excellent catalytic properties on the redox mediator process and electron transport has been studied to create a new development of DSSC [10-18]. According to Jinlong *et al.* [19], NiS_2 gives an excellent electrocatalytic activity and conductivity as a counter electrode. However, the efficiency obtained from NiS_2 CE is still uncompetitive as compared to the performance of Pt CE [20-22]. Therefore, in the present work, we studied the structural, electronic, and optical properties of NiS_2 and Fe-doped NiS_2 as counter electrode materials in DSSC.

COMPUTATIONAL METHOD

The first-principles calculations of NiS_2 and Fe-doped NiS_2 were performed using density functional theory (DFT) within Cambridge Serial Total Energy Package (CASTEP) computer code [23]. The exchange-correlation functional from local density approximation by Ceperley and Adler as

parametrised by Perdew and Zunger (LDA-CAPZ), generalised gradient approximation of Perdew-Burke-Ernzerhof (GGA-PBE) and Perdew-Burke-Ernzerhof for solids (GGA-PBEsol) were used. The structures of NiS_2 and Fe-doped NiS_2 were visualised in Figure 1. The NiS_2 and Fe-doped NiS_2 are cubic crystal structure with the space group of Pa-3 (205) (pyrite structure type) whereby the Ni atoms occupy the sites in face-centered cubic sublattice. In this work, the electron wave functions are expanded and converged in a standard plane-wave basis set with a kinetic energy cutoff of 350 eV. The calculations are performed using Monkhorst-Pack k-points meshes of $4 \times 4 \times 4$ with ultrasoft pseudopotential scheme. The bandgap using DFT usually underestimates the experimental bandgap. Thus, the DFT+U method has been used for electronic calculations [24-25]. The electronic properties calculations of NiS_2 were performed with and without Hubbard U (GGA-PBE+U) interaction and corrected with ($U = 3$ eV). All the calculations are performed based on the optimised lattice structure to get the structural properties (lattice parameters, volume, bond length), electronic properties (band structure, the density of states), and optical properties (dielectric function, refractive index, reflectivity, absorption coefficient, conductivity).

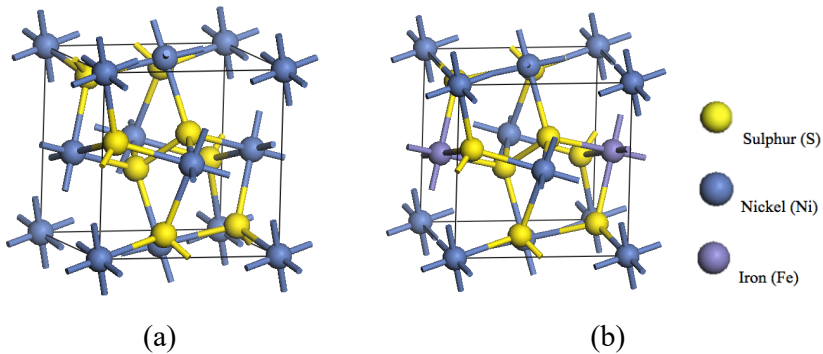


Figure 1: The Crystal Structures of (a) NiS_2 and (b) Fe-doped NiS_2

RESULTS AND DISCUSSION

Structural Properties

The lattice parameters and volumes from the full structural optimisation of NiS₂ and Fe-doped NiS₂ are listed in Table 1. The results indicated that the functional from GGA-PBE provides the best agreement with the experimental data [26-27], which have a relative deviation of 1.02% as compared to other functions. As for the Fe-doped NiS₂, it shows that the Fe doping does not alter the lattice constant that much due to the atomic radius of Fe and Ni is quite close [28]. The average bond length of the atoms in NiS₂ and Fe-doped NiS₂ was calculated by using GGA-PBE, which are presented in Table 2. The average bond length of the Ni-S bond is longer compared to the S-S bond.

Table 1: Lattice Parameters and Volumes of NiS₂ and Fe-doped NiS₂. Previous Experimental Data Also Included for Comparison

Structure	Functional	$a = b = c$ (Å)	V (Å ³)
NiS ₂	LDA-CAPZ	5.4688 (-3.79 %)	163.567 (-11.8 %)
	GGA-PBE	5.6194 (-1.02 %)	177.448 (-3.08 %)
	GGA-PBEsol	5.5228 (-2.78 %)	168.460 (-8.58 %)
	Experimental [23]	5.6765	182.912
Fe-doped NiS ₂	GGA-PBE	$a = 5.564176$	172.274
		$b = 5.565727$	
		$c = 5.563846$	

Table 2: Average Bond Length of NiS₂ and Fe-doped NiS₂

Material	Functional	S-S (Å)	Ni-S (Å)	Fe-S (Å)
NiS ₂	GGA-PBE	2.10346	2.36398	-
Fe-doped NiS ₂	GGA-PBE	2.13238	2.35072	2.26346

Electronic Properties

The DFT+U method was applied in the calculations by inserting the U parameter in 3d orbital of Ni atom to acquire an accurate estimation of U calculations. The U values were varied from 1 to 8 eV (Figure 2). The results in the band gaps concerning U show increasing bandgap as U values increase. The bandgap at U = 3 eV (0.384 eV) gives closest bandgap with the experimental values, $E_g = \sim 0.4$ eV [29]. To elucidate the nature of the electronic properties of NiS₂ and Fe-doped NiS₂, the correlation between electrons occupied orbital is illustrated by the density of states (DOS), as shown in Figure 3. The Fermi energy is presented at zero energy level. The DOS indicated no gap between the conduction band and valence band for both NiS₂ and Fe-doped NiS₂ due to the strong electron interaction of 3d orbital in the Ni atom. Hence this result demonstrates the characteristic of the structure of NiS₂ as a Mott-Hubbard correlated insulator [30]. The DOS shows that the valence band and conduction band are fully contributed by Ni 3d states, S 3p states, and the DOS of Fe-doped NiS₂ indicate the peaks of Ni 3d, S 3p, and Fe 3d states, respectively. After doping with Fe, the DOS show zero energy band gaps because of the highest valence band, and the lowest conduction band overlaps. Hence, Fe-doped NiS₂ behaves as a metallic material.

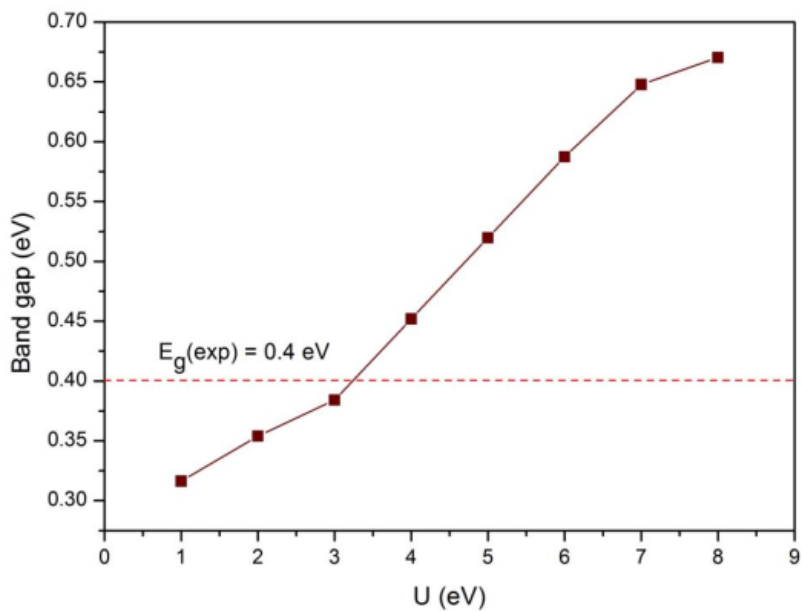
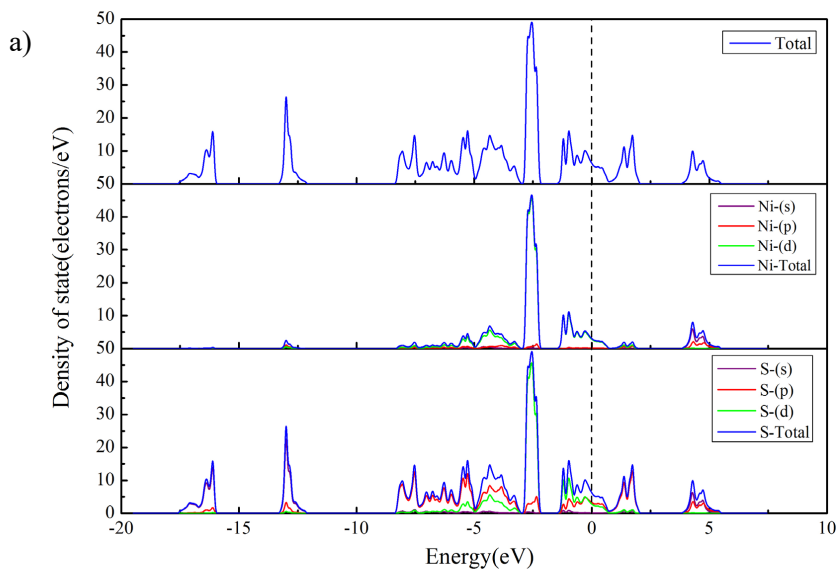
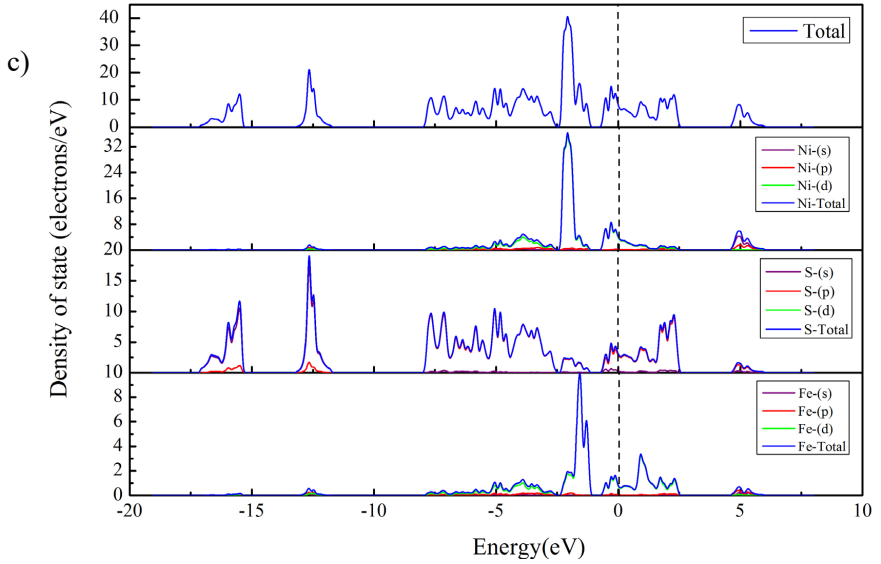
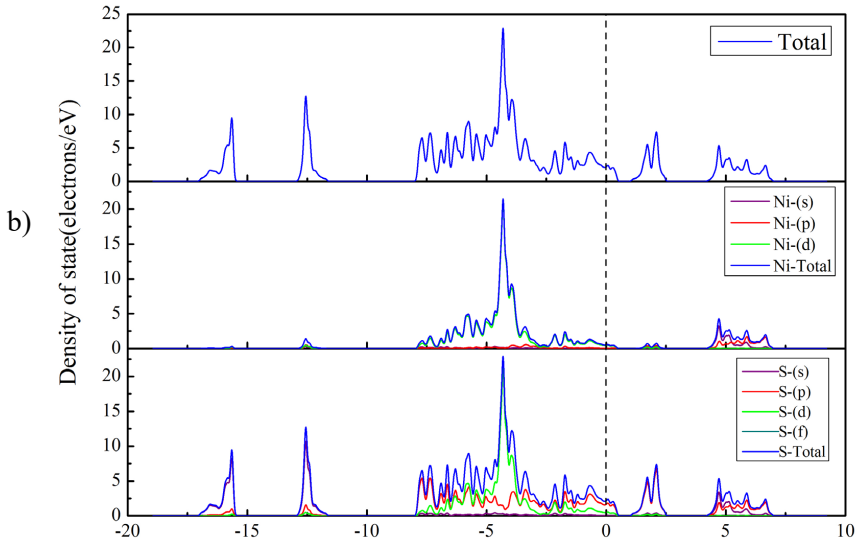


Figure 2: The Energy Bandgap Concerning Hubbard U from GGA-PBE+U, U = 1 to 8 eV





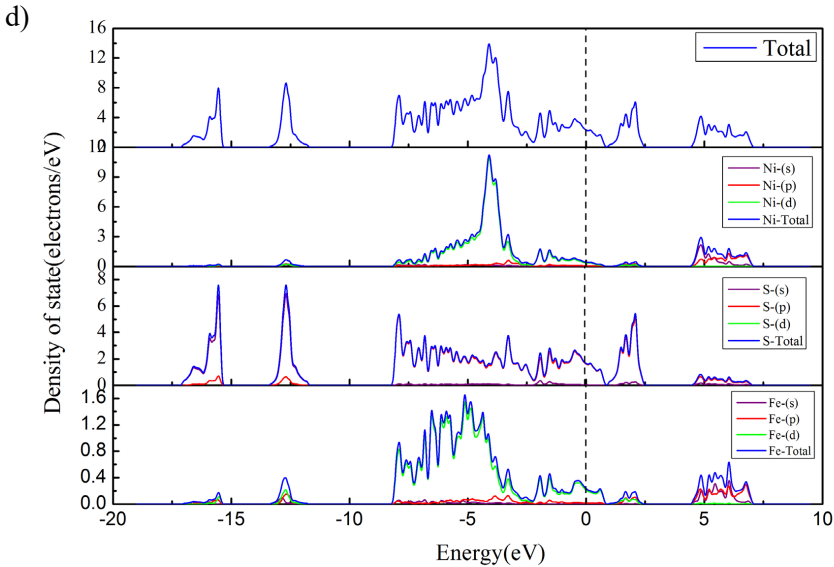


Figure 3: Density of States (DOS) of NiS₂ (a) Without U parameter, (b) with U Parameter and Fe-doped NiS₂ (c) Without U Parameter and (d) with U Parameter

Optical Properties

The optical properties of the dielectric function and refractive index of NiS₂ and Fe-doped NiS₂ are shown in Figure 4. The dielectric function, $\epsilon(\omega)$, and refractive index, $n(\omega)$, are observed up to 7000 nm. The dielectric function for the NiS₂ and Fe-doped NiS₂ at range 3000 nm up to 3500 nm (infrared region) shows the values of 32 and 40, respectively. This can be observed at the peak of the 3000 nm, whereby it shows that the Fe-doped NiS₂ has a greater dielectric function compared to the pure NiS₂. Meanwhile, in the visible region (300-700 nm), the pure NiS₂ shows a greater dielectric function as compared to Fe-doped NiS₂. The refractive index indicates the measurement of the ray light passes from a medium to another medium. The refractive index in Fe-doped NiS₂ exhibits higher value, which is 7.5 as compared to NiS₂ (6.1). Hence, both dielectric function and refractive index show that the Fe-doped NiS₂ has higher values in both properties, whereby these results may lead to greater performances of the efficiency in light-harvesting for DSSC.

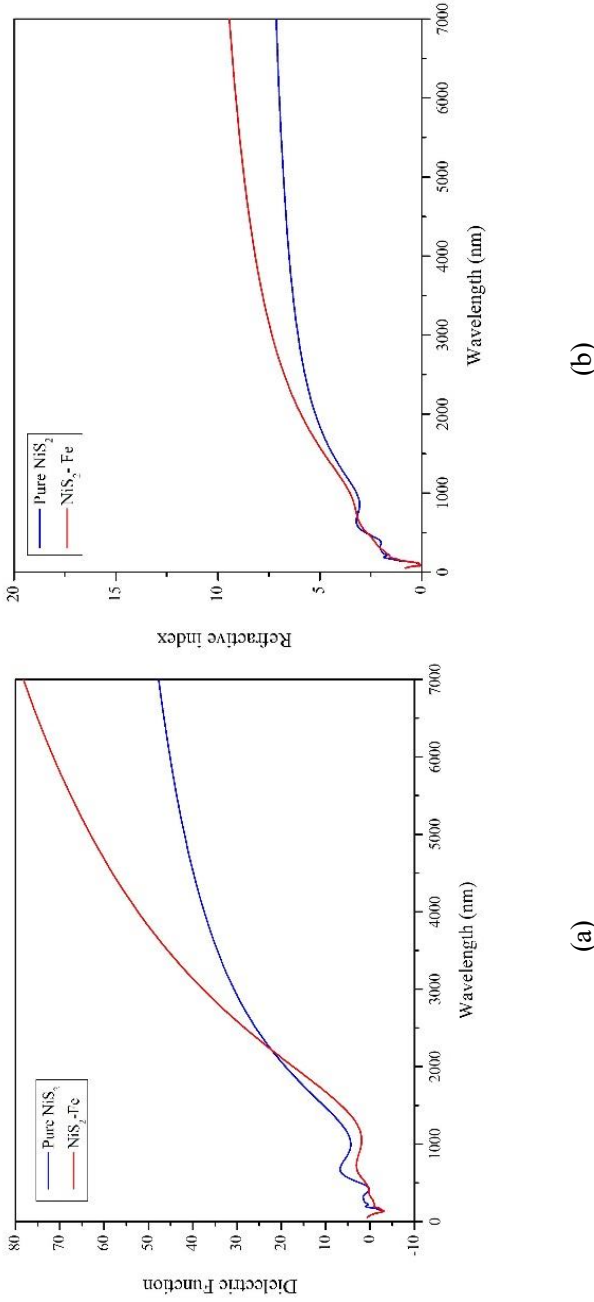
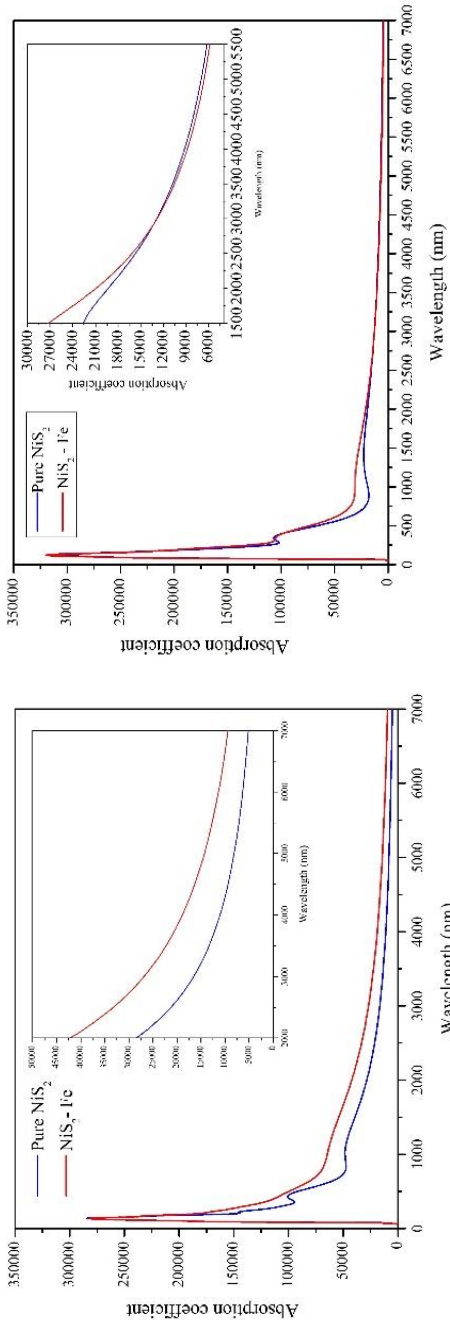


Figure 4: (a) Dielectric function and (b) Refractive index of NiS_2 and Fe-doped NiS_2 concerning wavelength (nm)

The absorption coefficient $\alpha(\omega)$ can determine the penetration of light into a material before it is absorbed. The calculated absorption coefficient of NiS₂ and Fe-doped NiS₂ without U and with U parameters are shown in Fig 5. The prominent peaks intensity for absorption values of NiS₂ and Fe-doped NiS₂ without U are $1.5 \times 10^4 \text{ cm}^{-1}$ and $2.5 \times 10^4 \text{ cm}^{-1}$, respectively, correspond to the wavelength of 3000 up to 3500 nm. As for the presence of the U parameter, the absorption coefficient has increased slightly to $2.25 \times 10^4 \text{ cm}^{-1}$ for NiS₂ and $2.55 \times 10^4 \text{ cm}^{-1}$ for Fe-doped NiS₂ in the region 1500 to 3000 nm. The optical absorption of the NiS₂ and Fe-doped NiS₂ at the infrared range (3000-3500 nm) corresponds to the bandgap obtained from the electronic properties.



(b)

(a)

Figure 5- Absorption Coefficient of NiS_2 and Fe-doped NiS_2 (a) Without U and (b) with U Parameter Concerning Wavelength (nm)

The reflectivity, $R(\omega)$, describes the amount of light reflected from the materials. The major peaks of the reflection spectra from reflectivity concerning wavelength of NiS_2 and Fe-doped NiS_2 are shown in Figure 6(a). In the infrared region, the Fe-doped NiS_2 exhibits greater reflectivity compared to NiS_2 . This result indicates that the Fe-doped NiS_2 has a higher reflection of light as compared to the pure NiS_2 . The conductivity is one of the important key mechanism for a counter electrode in DSSC. The optical conductivity in DSSC will indicate the electron charge transfer in the device system. The higher the conductivity will result in excellent performances of DSSC. Figure 6(b) shows that Fe-doped NiS_2 is slightly higher in conductivity concerning wavelength. The Fe-doped NiS_2 exhibits 3 fs^{-1} conductivity, which is higher than NiS_2 (1.5 fs^{-1}). Thus, due to the excellent conductivity obtained in Fe-doped NiS_2 , it can be concluded that the Fe-doped NiS_2 may provide an excellent electron charge transfer between the triiodide (I_3^-) and iodide (I^-) ions at the counter electrode, which can give higher efficiency of DSSC compare to pure NiS_2 .

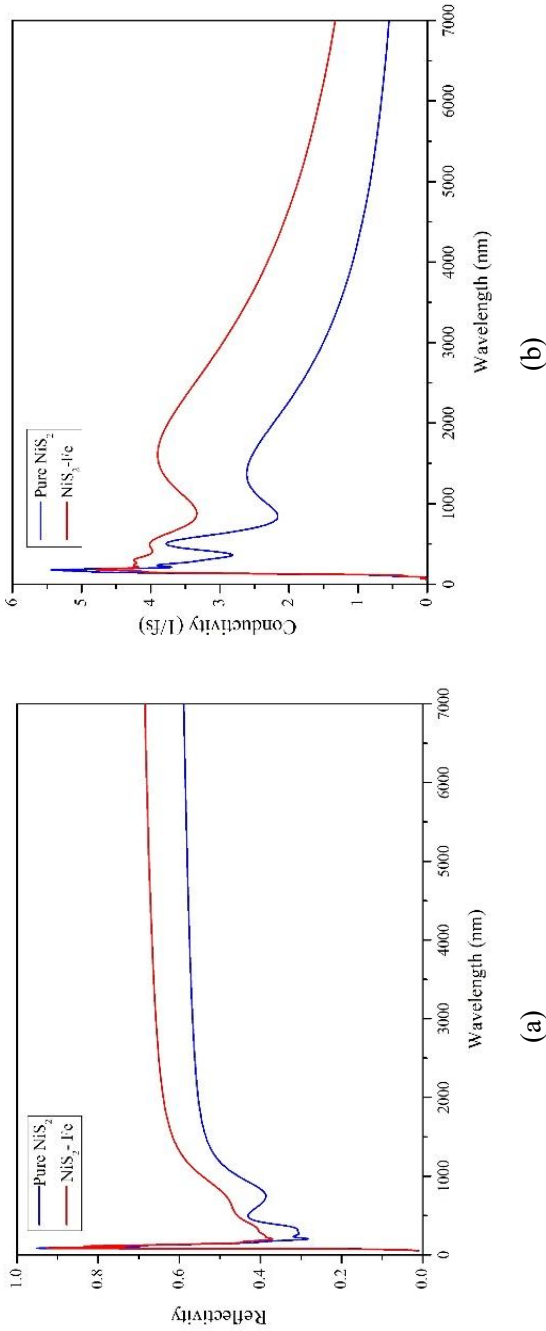


Figure 6: (a) Reflectivity and (b) Conductivity of NiS_2 and Fe-doped NiS_2 Against Wavelength (nm)

CONCLUSION

In summary, the structural, electronic, and optical properties of pure NiS₂ and Fe-doped NiS₂ are investigated in this work. The structural, electronic, and optical properties are calculated using GGA-PBE and the DFT+U from GGA-PBE+U to correct the strongly hybridised electrons in 3*d* and 3*p* orbitals. Analysis of the density of states (DOS) can be concluded that the hybridisation of the electron takes place at S 2*s* at the valence band and Ni 3*d* together with S 3*p* and Fe 3*d* for both pure NiS₂ and Fe-doped NiS₂. As for optical properties, the results show the enhancement of the doped material as compared to the pure NiS₂. The conductivity exhibits a good result for electron transfer. Hence, it may give good improvement for the counter electrode in DSSC.

ACKNOWLEDGEMENT

The authors would like to thank the Ministry of Higher Education (MOHE) Malaysia for funding this research under the FRGS grant 600-IRMI/FRGS 5/3 (337/2019) and Universiti Teknologi MARA (UiTM) for the facilities provided.

REFERENCES

- [1] J. Gong, J. Liang, & K. Sumathy, 2012. Review on dye-sensitized solar cells (DSSCs): fundamental concepts and novel materials. *Renewable and Sustainable Energy Reviews*, 16(8), 5848-5860. <https://doi.org/10.1016/j.rser.2012.04.044>
- [2] M. Grätzel, 2003. Dye-sensitized solar cells. *Journal of Photochemistry and Photobiology C: Photochemistry Reviews*, 4(2), 145-153. [https://doi.org/10.1016/S1389-5567\(03\)00026-1](https://doi.org/10.1016/S1389-5567(03)00026-1)
- [3] M. Ye, X. Wen, M. Wang, J. Iocozzia, N. Zhang, C. Lin, & Z. Lin, 2015. Recent advances in dye-sensitized solar cells: from photoanodes,

- sensitizers and electrolytes to counter electrodes. *Materials Today*, 18(3), 155-162. <https://doi.org/10.1016/j.mattod.2014.09.001>
- [4] S. Sharma, K. K. Jain, & A. Sharma, 2015. Solar cells: In research and applications - a review. *Materials Sciences and Applications*, 6(12), 1145. DOI: 10.4236/msa.2015.612113
- [5] J. Wu, Z. Lan, J. Lin, M. Huang, Y. Huang, L. Fan, G. Luo, Y. Lin, Y. Xie, Y. Wei, 2017. Counter electrodes in dye-sensitized solar cells. *Chemical Society Reviews*, 46(19), 5975-6023. <https://doi.org/10.1039/C6CS00752J>
- [6] W. Priani, F. Nurosyid, & R. Suryana, 2019. The effect of Pt-counter electrode deposition methods on the efficiency of Dye-Sensitized Solar Cells. *Journal of Physics: Conference Series*, Volume 1153, 9th International Conference on Physics and Its Applications (ICOPIA) 14 August 2018, Surakarta, Indonesia
- [7] C. P., Lee, C. T Li, & K.C. Ho, 2017. Use of organic materials in dye-sensitized solar cells. *Materials Today*, 20(5), 267-283. <https://doi.org/10.1016/j.mattod.2017.01.012>
- [8] G. Syrokostas, A. Siokou, G. Leftheriotis, & P. Yianoulis, 2012. Degradation mechanisms of Pt counter electrodes for dye sensitized solar cells. *Solar Energy Materials and Solar Cells*, 103, 119-127. <https://doi.org/10.1016/j.solmat.2012.04.021>
- [9] A. Hauch, & A. Georg, 2001. Diffusion in the electrolyte and charge-transfer reaction at the platinum electrode in dye-sensitized solar cells. *Electrochimica Acta*, 46(22), 3457-3466. [https://doi.org/10.1016/S0013-4686\(01\)00540-0](https://doi.org/10.1016/S0013-4686(01)00540-0)
- [10] J. Theerthagiri, A. R. Senthil, Madhavan, J., & Maiyalagan, T. (2015). Recent Progress in Non-Platinum Counter Electrode Materials for Dye-Sensitized Solar Cells. *ChemElectroChem*, 2(7), 928-945. <https://doi.org/10.1002/celec.201402406>

- [11] S. Xu, Y. Luo, & W. Zhong, 2011. Investigation of catalytic activity of glassy carbon with controlled crystallinity for counter electrode in dye-sensitized solar cells. *Solar energy*, 85(11), 2826-2832. <https://doi.org/10.1016/j.solener.2011.08.014>
- [12] X. Yin, F. Wu, N. Fu, J. Han, D. Chen, P. Xu, M. He, Y. Lin, 2013. Facile synthesis of poly (3, 4-ethylenedioxythiophene) film via solid-state polymerization as high-performance Pt-free counter electrodes for plastic dye-sensitized solar cells. *ACS Applied Materials & Interfaces*, 5(17), 8423-8429.
- [13] M. Wu, Y. Wang, X. Lin, N. Yu, L. Wang, L. Wang, A. Hagfeldt, T. Ma, 2011. Economical and effective sulfide catalysts for dye-sensitized solar cells as counter electrodes. *Physical Chemistry Chemical Physics*, 13(43), 19298-19301. <https://doi.org/10.1039/C1CP22819F>
- [14] J. Y. Lin, & S. W. Chou, 2013. Highly transparent NiCo₂S₄ thin film as an effective catalyst toward triiodide reduction in dye-sensitized solar cells. *Electrochemistry Communications*, 37, 11-14. <https://doi.org/10.1016/j.elecom.2013.09.027>
- [15] I. A. Ji, H. M. Choi, & J. H. Bang, 2014. Metal selenide films as the counter electrode in dye-sensitized solar cell. *Materials Letters*, 123, 51-54. <https://doi.org/10.1016/j.matlet.2014.02.080>
- [16] N. Balis, V. Dracopoulos, K. Bourikas, & P. Lianos, 2013. Quantum dot sensitized solar cells based on an optimized combination of ZnS, CdS and CdSe with CoS and CuS counter electrodes. *Electrochimica Acta*, 91, 246-252. <https://doi.org/10.1016/j.electacta.2013.01.004>
- [17] H. Kim, H. Choi, S. Hwang, Y. Kim, & M. Jeon, 2012. Fabrication and characterization of carbon-based counter electrodes prepared by electrophoretic deposition for dye-sensitized solar cells. *Nanoscale Research Letters*, 7(1), 53. <https://doi.org/10.1186/1556-276X-7-53>
- [18] M.H. Samat, M.F.M. Taib, O.H. Hassan, *et al.*, 2020. First-principles study on XV₂S₄ (X = Ni, Cr, and Mo) counter electrode for dye-sensitized solar cells. *Emergent Mater*, 3, 125–131. <https://doi.org/10.1007/s42247-020-00089-y>

- [19] Jinlong Zheng, Z. G., Wei Zhou, Rongzun Zhang, Junxiang Wang, Yuzun Fan, Rui Zhang, Zhimei Sun, 2018. Synergistic effect of Ni and Fe in Fe-doped NiS₂ counter electrode for dye-sensitized solar cells- Experimental and DFT studies. *Electrochimica Acta*, 284, 24-29. DOI:10.1016/j.electacta.2018.07.138
- [20] Z. Wan, C. Jia, & Y. Wang, 2015. In situ growth of hierarchical NiS₂ hollow microspheres as efficient counter electrode for dye-sensitized solar cell. *Nanoscale*, 7(29), 12737-12742. DOI:10.1039/c5nr03054d
- [21] X. Yang, L. Zhou, A. Feng, H. Tang, H. Zhang, Z. Ding, Y. Ma, M. Wu, S. Jin & G. Li, 2014. Synthesis of nickel sulfides of different phases for counter electrodes in dye-sensitized solar cells by a solvothermal method with different solvents. *Journal of Materials Research*, 29(8), 935-941. <https://doi.org/10.1557/jmr.2014.74>
- [22] J. Zheng, W. Zhou, Y. Ma, W. Cao, C. Wang, & L. Guo, 2015. Facet-dependent NiS₂ polyhedrons on counter electrodes for dye-sensitized solar cells. *Chemical Communications*, 51(64), 12863-12866. <https://doi.org/10.1039/C5CC03890A>
- [23] M. D. Segall, P. J. D. Lindan, M. J. Probert, C. J. Pickard, P. J. Hasnip, S. J. Clark, & M. C. Payne, 2002. First-principles simulation: Ideas, illustrations and the CASTEP code. *Journal of Physics: Condensed Matter*, 14(11), 2717.
- [24] M. H. Samat, A. M. M. Ali, M. F. M. Taib, O. H. Hassan, & M. Z. A. Yahya, 2016. Hubbard U calculations on optical properties of 3d transition metal oxide TiO₂. *Results in Physics*, 6(2016), 891-896. <https://doi.org/10.1016/j.rinp.2016.11.006>
- [25] M. H. Ridzwan, M. K. Yaakob, M. F. M. Taib, A. M. M. Ali, O. H. Hassan, & M. Z. A. Yahya, 2017. Investigation of structural, electronic and optical properties of hexagonal LuFeO₃ using first principles LDA+U. *Materials Research Express*, 4(4), 044001. DOI: 10.1088/2053-1591/aa65b5

- [26] S. Liu, Y. Li, J. Liu, & Y. Shi, 2015. First-principles study of sulfur isotope fractionation in pyrite-type disulfides. *American Mineralogist*, 100(1), 203-208. <https://doi.org/10.2138/am-2015-5003>
- [27] N. X. Miao, Y. X. Lei, J. P. Zhou, & Q. U. Hassan, 2018. Theoretical and experimental researches on NiS₂ nanocubes with uniform reactive exposure facets. *Materials Chemistry and Physics*, 207, 194-202. <https://doi.org/10.1016/j.matchemphys.2017.12.026>
- [28] T. Wang, X. Guo, J. Zhang, W. Xiao, P. Xi, S. Peng, & D. Gao, 2019. Electronic structure modulation of NiS₂ by transition metal doping for accelerating the hydrogen evolution reaction. *Journal of Materials Chemistry A*, 7(9), 4971-4976. <https://doi.org/10.1039/C8TA11286J>
- [29] N. Jiang, Q. Tang, M. Sheng, B. You, D. E. Jiang, & Y. Sun, 2016. Nickel sulfides for electrocatalytic hydrogen evolution under alkaline conditions: A case study of crystalline NiS, NiS₂, and Ni₃S₂ nanoparticles. *Catalysis Science & Technology*, 6(4), 1077-1084. <https://doi.org/10.1039/C5CY01111F>
- [30] Y. Feng, R. Jaramillo, A. Banerjee, J. M. Honig, & T. F. Rosenbaum, 2011. Magnetism, structure, and charge correlation at a pressure-induced Mott-Hubbard insulator-metal transition. *Physical Review B*, 83(3), 035106. DOI: 10.1103/PhysRevB.83.035106